Journal of Materials Chemistry A

ROYAL SOCIETY OF CHEMISTRY

PAPER

View Article Online
View Journal | View Issue

Cite this: J. Mater. Chem. A, 2024, 12, 30548

Advancing energy safety *via* stepwise nucleophilic substitution on tetrazine†

Jatinder Singh, [a] Richard J. Staples [b] and Jean'ne M. Shreeve *[a]

Historically hydrazine (N_2H_4) has served an essential function as a fuel in liquid rocket propellants; however, its intrinsic volatility and toxicity pose significant challenges in fulfilling the requirements for environmentally friendly and high-performance propellants. Introducing hydrazine onto a nitrogen-rich framework offers the possibility to use it as solid-rocket propellant. Now for the first time both hydrazine and nitroamine groups, energetic small groups, were introduced onto a tetrazine ring through stepwise functionalization. *N*-(6-(3,5-Dimethyl-1*H*-pyrazol-1-yl)-1,2,4,5-tetrazin-3-yl)nitramide (**3**) serves as an energetic intermediate, which upon reaction with hydrazine or ammonia results in the synthesis of unsymmetrically substituted tetrazine derivatives (**4** and **8**) *via* nucleophilic substitution and salt formation (a domino or cascade reaction). Compounds **5** and **9** (salts of **4** and **8**, respectively) exhibit detonation properties on a par with RDX, providing the added benefits of high nitrogen content and reduced sensitivity, and **7** and **11** (neutral derivatives of **4** and **8**, respectively) show promising propulsive properties, highlighting their potential as solid rocket propellants. This research will significantly advance the synthesis of unsymmetrically substituted tetrazines, enabling precise control over their energetic properties.

Received 26th August 2024
Accepted 15th October 2024

DOI: 10.1039/d4ta06039c

rsc.li/materials-a

1. Introduction

The advantage of sequential unsymmetric substitution reactions in organic chemistry lies in the versatility for creating diverse molecules with specific functionalities.[1] This diversity expands the range of molecules that can be synthesized, enabling the development of new materials, pharmaceuticals, agrochemicals, and other useful compounds.[2] For energetic materials, unsymmetric substitution reactions allow for selective introduction of various functional groups onto a molecule.[3] As research in energetic materials advances, nitrogen-rich compounds offer significant potential for developing more powerful, insensitive, and environmentally friendly explosives, propellants, pyrotechnics, and oxidizers, making them particularly promising for emerging applications.[4–10] Specifically, pyrazole, triazole, and tetrazole rings have garnered considerable interest due to their remarkably high nitrogen content.[10–20] Notable examples include ANTA (3-amino-5-nitro-1,2,4-triazole), HDNT (3,5-dinitro-1,2,4-triazole), and TKX-50 (dihydroxylammonium 5,5′-bistetrazole-1,1′-diolate).[21–23] Due to the vastly increasing interest in energetic materials and their applicability in defense and civilian industries, the need for high energy density and environmental compatibility has never been greater.

Tetrazine, a six-membered heterocyclic ring with four nitrogen atoms, is highly sought after as energetic materials not only because of their nitrogen content but accessibility.[24–29] The most prevalent method for preparing symmetric tetrazines involves cyclization of two nitrile molecules to form a 1,4-dihydro-*s*-tetrazine precursor, which is then typically oxidized using a nitrous reagent. Similarly, symmetric tetrazines can also be obtained through the reaction of 1,2-diketones with hydrazine. Over the years researchers have demonstrated that 3,6-bis(3,5-dimethyl-1*H*-pyrazol-1-yl)-1,2,4,5-tetrazine (**1**), obtained from a later method,[30] serves as a crucial precursor in the synthesis of nitrogen-rich energetic compounds. Its C3 and C6 sites are highly reactive, which enables straightforward substitution by nucleophiles to yield diverse derivatives (Fig. 1).

While nucleophilic substitution on 3,6-bis(3,5-dimethyl-1*H*-pyrazol-1-yl)-1,2,4,5-tetrazine is well-documented, exploration of stepwise selective unsymmetric functionalization remains limited.[31–36] Previous methods for obtaining compounds such as 3-amino-6-nitroaminotetrazine (ANAT) and *N*,*N*′-(1,2,4,5-tetrazine-3,6-diyl)dinitramide involve drawbacks such as requiring high temperatures (140 °C) and pressures (liquid NH_3 in a steel vessel) during the synthesis of 1,2,4,5-tetrazine-3,6-diamine (Fig. 2).

Recently, the utility of compound (**1**) has been demonstrated in the synthesis of fused energetic materials (Fig. 2). A notable strategy involves cyclization reactions between hydrazine (NH_2–

[a]Department of Chemistry, University of Idaho, Moscow, Idaho, 83844-2343, USA. E-mail: jshreeve@uidaho.edu; Fax: +1-208-885-5173

[b]Department of Chemistry, Michigan State University, East Lansing, Michigan 48824, USA

† Electronic supplementary information (ESI) available: Synthesis of compounds, isodesmic reactions, characterization data. CCDC 2378050 (**5**); 2378051 (**9**·H_2O); 2378052 (**11**). For ESI and crystallographic data in CIF or other electronic format see DOI: https://doi.org/10.1039/d4ta06039c

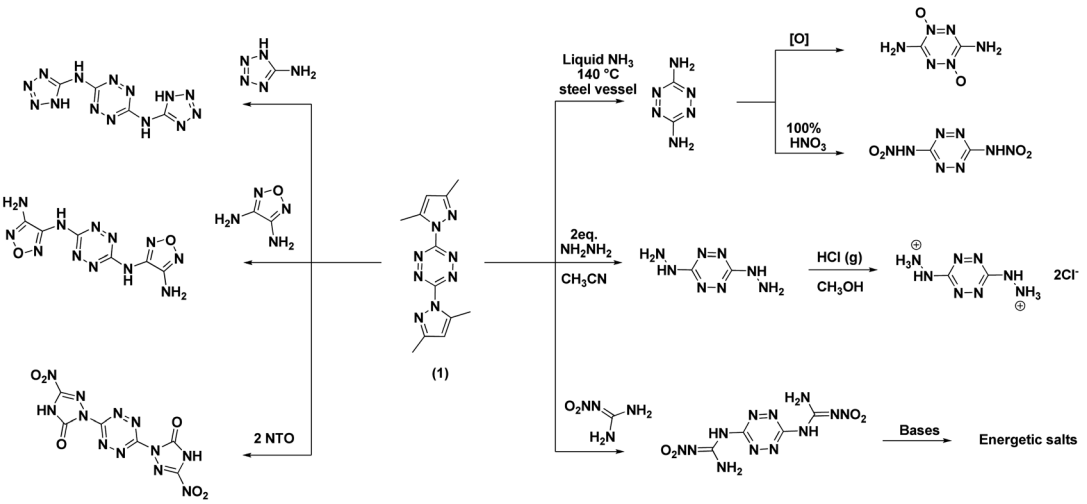

Fig. 1 Representative examples for symmetrically substituted tetrazine derivatives.

NH_2) and cyanogen bromide to produce triazolo-triazine fused derivatives.[37–39] Given the broad range of energetic materials that can be obtained through asymmetric substitution and their potential applications, there is a need for alternate approaches. In this study, we have synthesized new unsymmetric substituted tetrazine derivatives through the stepwise functionalization of 3,6-bis(3,5-dimethyl-1*H*-pyrazol-1-yl)-1,2,4,5-tetrazine using a straightforward approach. The aim of the method is to identify more advanced energetic compounds with further optimized properties (Fig. 3).

2. Results and discussion

2.1. Synthesis

3,6-Bis(3,5-dimethyl-1*H*-pyrazol-1-yl)-1,2,4,5-tetrazine (**1**), 6-(3,5-dimethyl-1*H*-pyrazol-1-yl)-1,2,4,5-tetrazin-3-amine (**2**), and *N*-(6-(3,5-dimethyl-1*H*-pyrazol-1-yl)-1,2,4,5-tetrazin-3-yl)nitramide (**3**) were synthesized following established literature procedures.[34] The reaction of **3** with $N_2H_4 \cdot H_2O$ (98%, 2 equivalents) in ethanol at 0 °C resulted in nucleophilic substitution and salt formation (a cascade reaction) to yield compound **4** as a single product (Scheme 1). Notably, the reaction of **3** with excess $N_2H_4 \cdot H_2O$ (98%, 4 equivalents) in ethanol at room temperature resulted only in the formation of 3,6-dihydrazinyl-1,2,4,5-tetrazine (Scheme 1). The reaction of compound **4** with $AgNO_3$ was unsuccessful, as the resulting red solid decomposed rapidly after formation. Compounds **5** and **6** were obtained from compound **4** owing to their low solubility in water. Compound **4** was neutralized effectively with 10% H_2SO_4, producing **7** in quantitative yield (Scheme 1).

Compound **8** was previously obtained by the reaction of 3-amino-6-nitroaminotetrazine[33] (ANAT) with aqueous ammonia (Fig. 2). Here, it was formed by using not only compound **3** and aq. ammonia but with *N*,*N*′-(1,2,4,5-tetrazine-3,6-diyl)

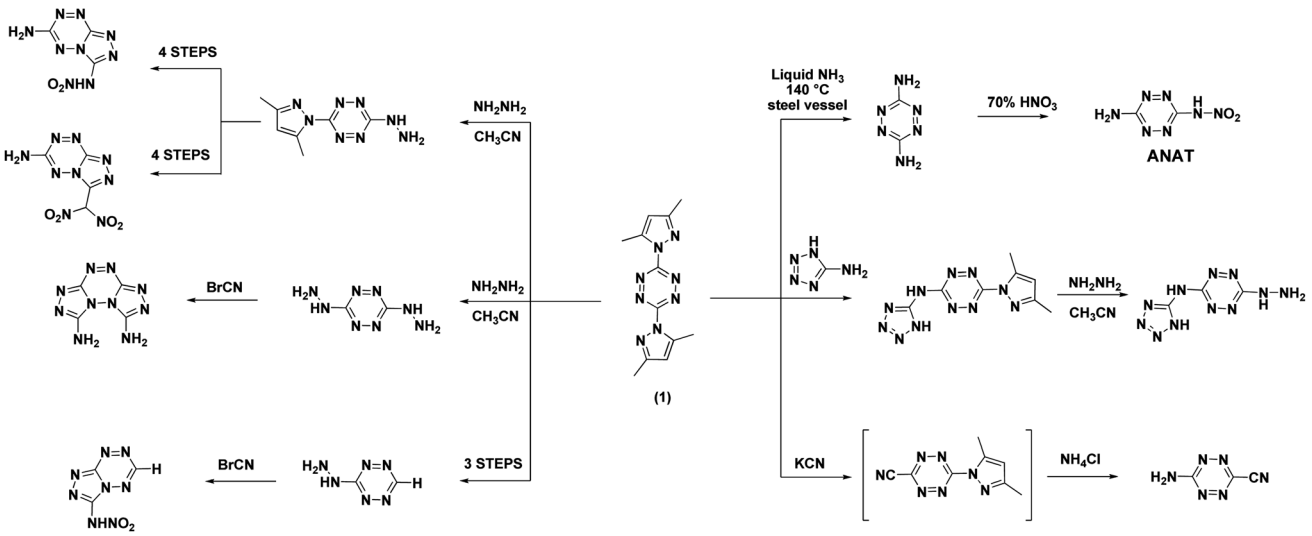

Fig. 2 Representative examples for tetrazine-based asymmetrical and fused energetic materials.

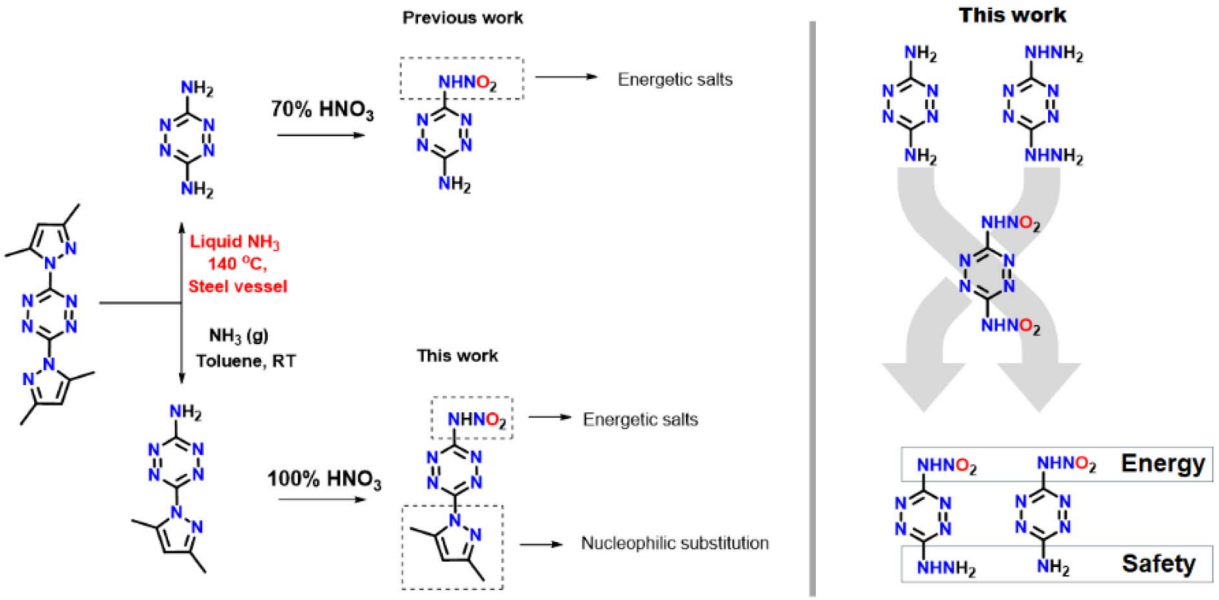

Fig. 3 Previous work and present work.

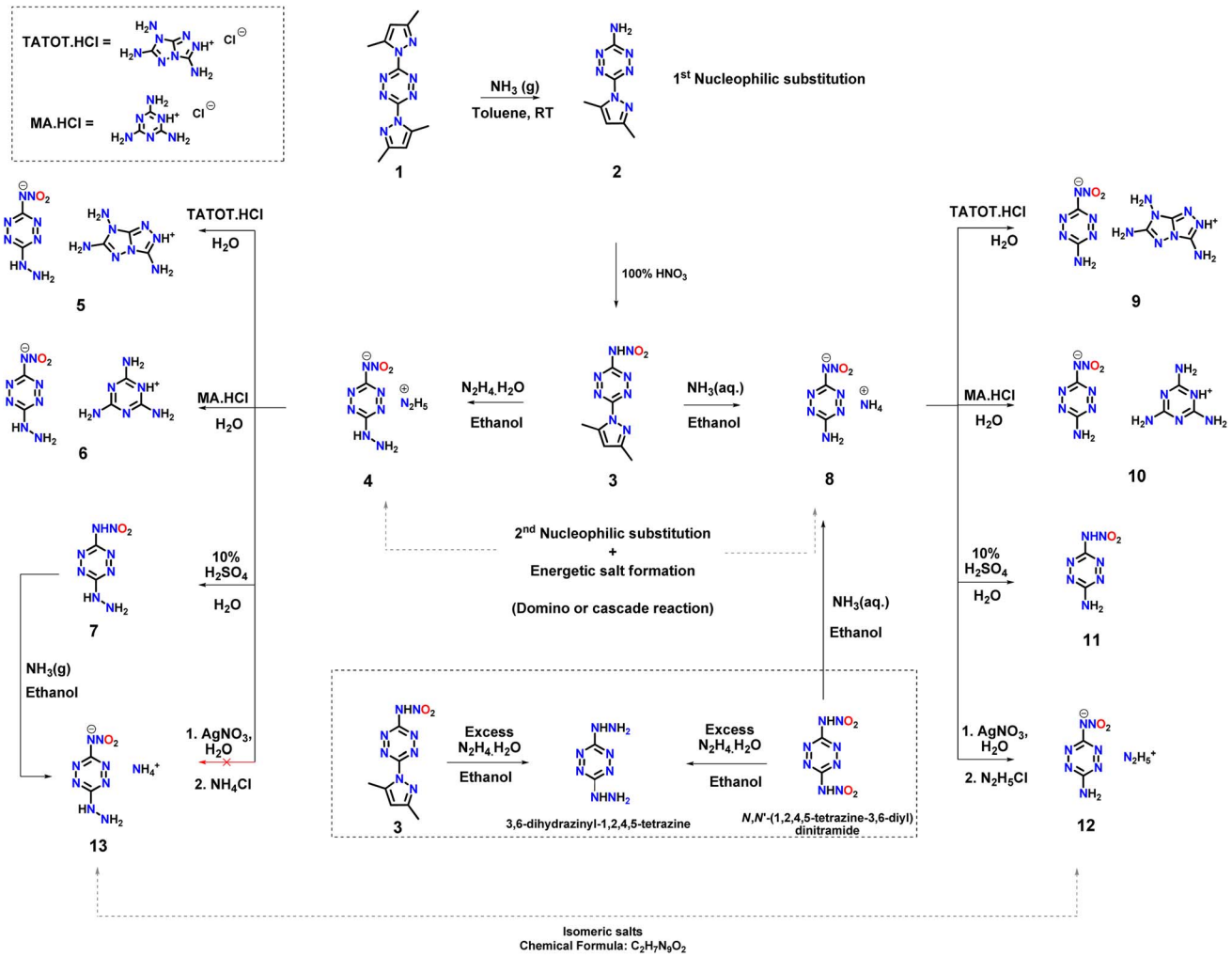

Scheme 1 Synthesis of compounds 4–13.

dinitramide and aq. ammonia (Scheme 1). Salts **9** and **10** were obtained directly from **8** in quantitative yields by taking advantage of their low solubility in water. Compound **8** was neutralized effectively with 10% H_2SO_4, producing **11** in quantitative yield (Scheme 1). In contrast to compound **4**, the reaction of compound **8** with $AgNO_3$ followed by $N_2H_5 \cdot Cl$ results in hydrazinium salt **12**. Compound **7** was reacted with gaseous NH_3 in ethanol to yield **13**.

2.2. NMR spectroscopy

All new compounds were characterized by NMR spectroscopy. In the ^{13}C NMR spectrum of compound **4**, two peaks for C1 and C2 were observed at 163.8 ppm and 162.2 ppm, respectively (Fig. 4A). Upon neutralization with acid to form **7**, these two carbon peaks were shifted upfield to 161.1 ppm and 160.1 ppm, respectively (Fig. 4B). In compound **8**, C1 and C2 were observed at 163.4 ppm and 161.9 ppm, respectively (Fig. 4C). After neutralization with acid to form **11**, the two carbon peaks were shifted upfield to 162.5 ppm and 154.7 ppm, respectively (Fig. 4D). The chemical environments of different nitro groups were determined using ^{14}N NMR (Fig. 4E and F). Given the high nitrogen content of all the compounds, the ^{15}N NMR spectra of selected compounds were recorded also (Fig. 4G and H). In case of **11**, the NH_2 signal is seen at 269.3 ppm.

2.3. Crystal structure

Single crystals of compound **5** suitable for X-ray analysis were obtained by slow evaporation from methanol : water (1 : 1) mixtures. It crystallizes in a triclinic ($P\bar{1}$) space group. The crystal structure supports the presence of one nitramide anion and one TATOT cation, resulting in the molecular formula $C_5H_{10}N_{16}O_2$, with a density of 1.798 g cm^{-3} at 100 K (ESI, Section S2†). Notably, the nitrogen and oxygen atoms of the anion form strong hydrogen bonds with the surrounding TATOT cations, with bond lengths ranging from 1.88 Å to 2.25 Å (Fig. 5A–C). Compound **5** has planar stacking with layer spacing of 3.3 Å, lower than that of (3.65–4.00 Å) common aromatic π–π interactions. The interlayer spacing suggests that there may be strong π–π interactions between the molecules.

Single crystals of compound **9** suitable for X-ray analysis were obtained by slow evaporation from methanol : water (1 : 1) mixtures. It crystallizes in a triclinic ($P\bar{1}$) space group with one

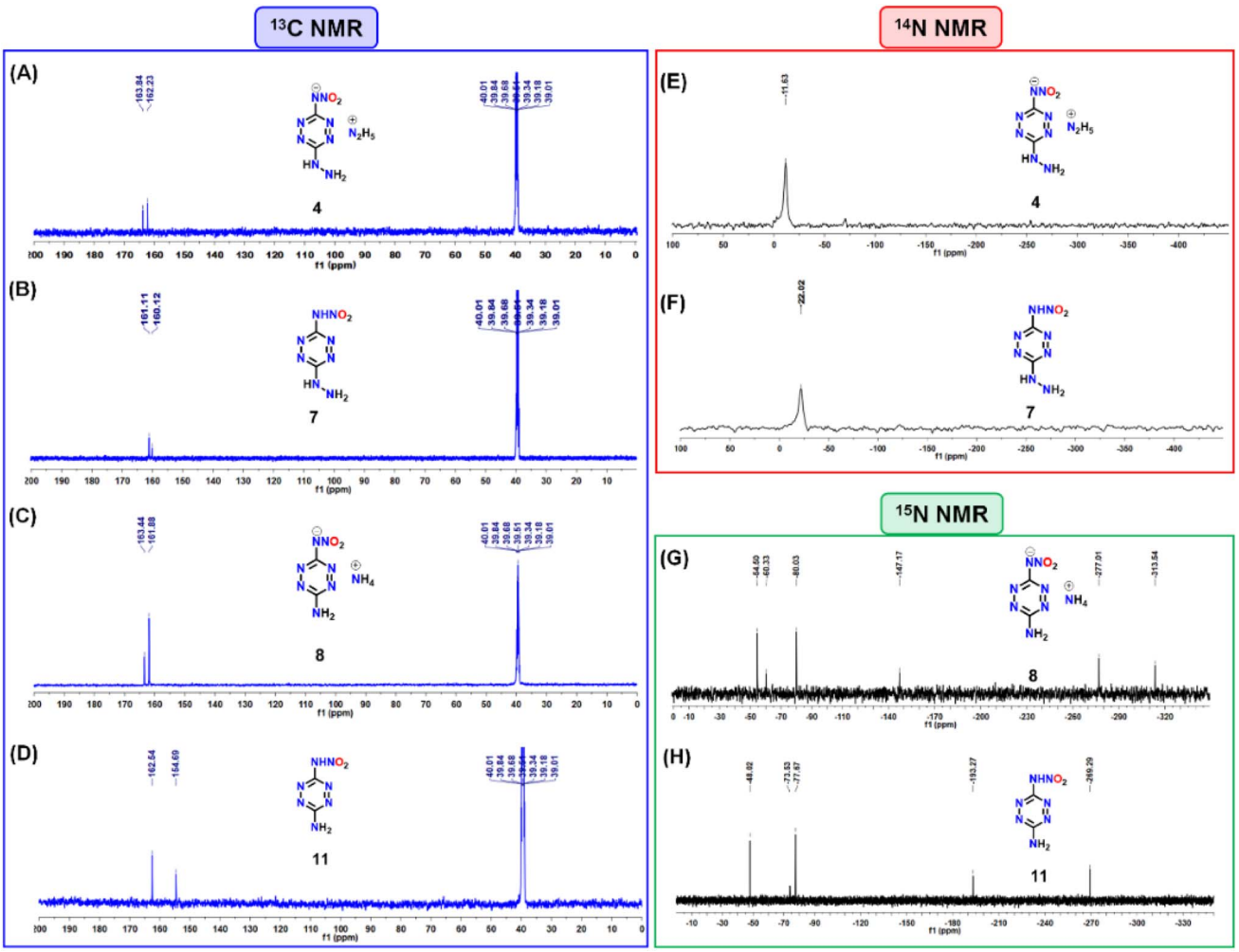

Fig. 4 ^{13}C NMR of (A) **4**. (B) **7**. (C) **8**. (D) **11**. ^{14}N NMR of (E) **4**. (F) **7**. ^{15}N NMR of (G) **8**. (H) **11**.

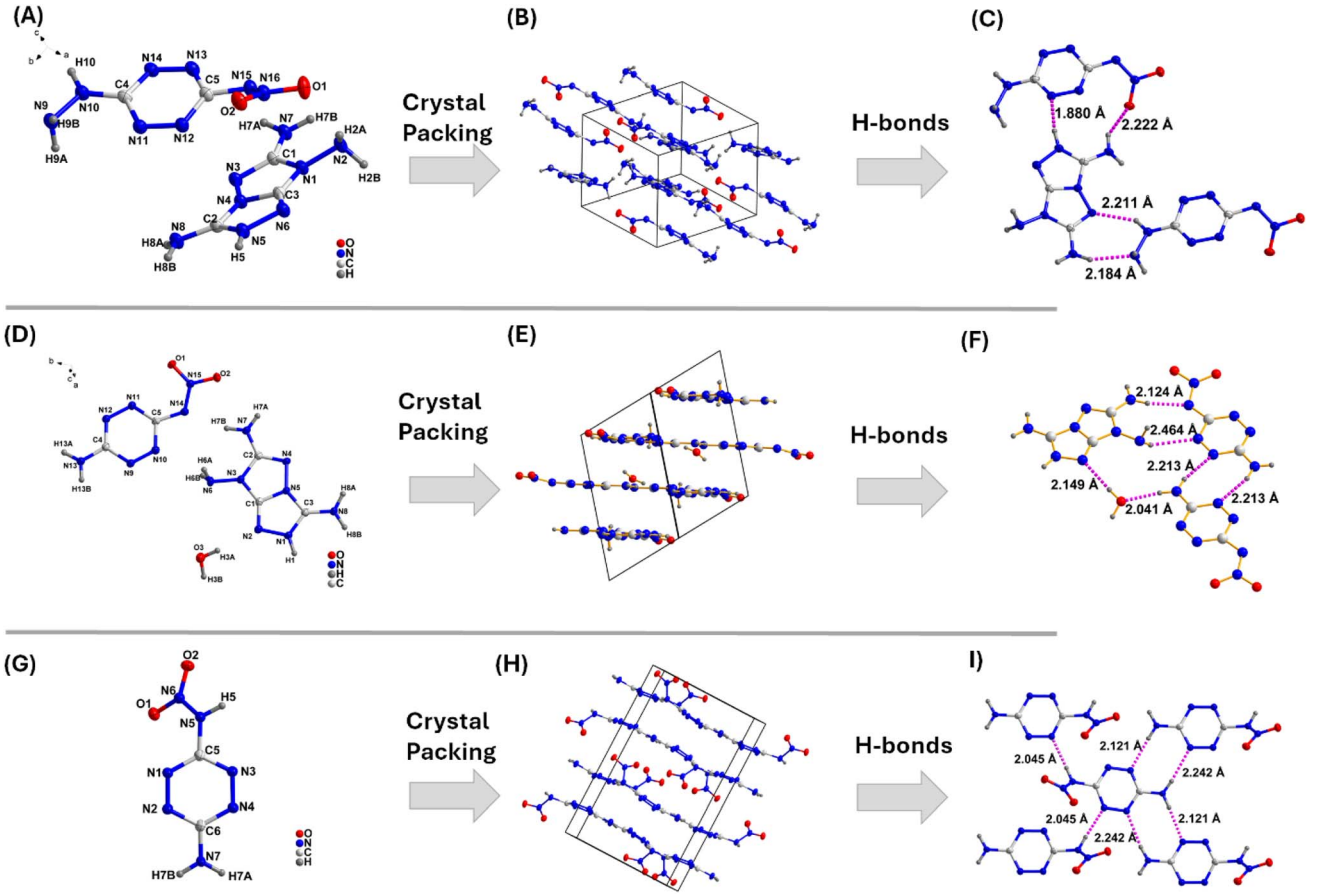

Fig. 5 (A) Tagging scheme of **5**. (B) Packing diagram of **5**. (C) Hydrogen bond networks in **5**. (D) Tagging scheme of **9**·H_2O. (E) Packing diagram of **9**·H_2O. (F) Hydrogen bond networks in **9**·H_2O. (G) Tagging scheme of **11**. (H) Packing diagram of **11**. (I) Hydrogen bond networks in **11**.

water molecule in the crystal lattice as **9**·H_2O. The crystal structure comprises one nitramide anion and one TATOT cation, resulting in the molecular formula $C_5H_9N_{15}O_2 \cdot H_2O$, with a density of 1.805 g cm^{-3} at 100 K (ESI, Section S2†). Notably, the nitrogen and oxygen atoms of the anion form strong hydrogen bonds with the surrounding TATOT cations, forming bonds with lengths ranging from 1.85 Å to 2.47 Å (Fig. 5D–F). In **9**·H_2O, planar stacking of tetrazine and TATOT rings is also seen (Fig. 5E). The interlayer spacing between the rings is 3.1 Å, indicating strong π–π interactions. The packing index is calculated to be 77.4%. Despite having one water molecule in the crystal lattice, it exhibits good density owing to the planar packing and strong O···H/H···O and N···H/H···N bond networks.

Single crystals of compound **11** suitable for X-ray analysis were obtained by slow evaporation from methanol : water (1 : 1) mixtures. It crystallizes in an orthorhombic (*Pbca*) space group and is comprised of a tetrazine ring substituted with one amino and one nitroamino group, resulting in the molecular formula $C_2H_3N_7O_2$, with a density of 1.868 g cm^{-3} at 100 K (ESI, Section S2†). The intermolecular hydrogen bond lengths between molecules range from 2.05 Å to 2.12 Å (Fig. 5G–I). The packing index is calculated to be 76.6%. The packing diagram reveals planar packing with strong O···H/H···O and N···H/H···N bond networks, which contribute to high density and good stability.

2.4. Physicochemical properties

High thermal stability is crucial for useful energetic materials. Thermal characteristics were determined using differential scanning calorimetry (DSC) analysis at the heating rate of 5 °C and 10 °C min^{-1} (Fig. 6). At 5 °C min^{-1}, the decomposition of energetic salt **5** occurs at 159 °C (onset) (Fig. 6A). For compound **7**, the onset decomposition is found at 139 °C (Fig. 6B). For **9** and **10**, the decomposition temperatures are at 241 °C (onset) and 252 °C (onset), respectively (Fig. 6C and D). For compound **11**, the onset thermal decomposition occurs at 175 °C (Fig. 6E). For **13**, the decomposition occurs at 123 °C (onset) (Fig. 6F).

To study structure–property relationships, in-depth exploration of weak interactions was conducted *via* Hirshfeld surface and 2D fingerprint analyses.[40,41] The red regions on the Hirshfeld surfaces indicate interactions between neighboring molecules. For compound **5**, four tiny spikes were observed in the 2D fingerprint plot, representing O···H/H···O and N···H/H···N hydrogen bond interactions (Fig. 7B). The total calculated populations of stabilizing O···H/H···O and N···H/H···N interactions in compound **5** are 21% and 42%, respectively. The π–π interactions resulting from stacking of the anion and cations can be visualized by displaying non-covalent interaction plots (Fig. 7C).

Similarly for compounds **9**·H_2O and **11**, spikes were observed in the 2D fingerprint plot, representing O···H/H···O

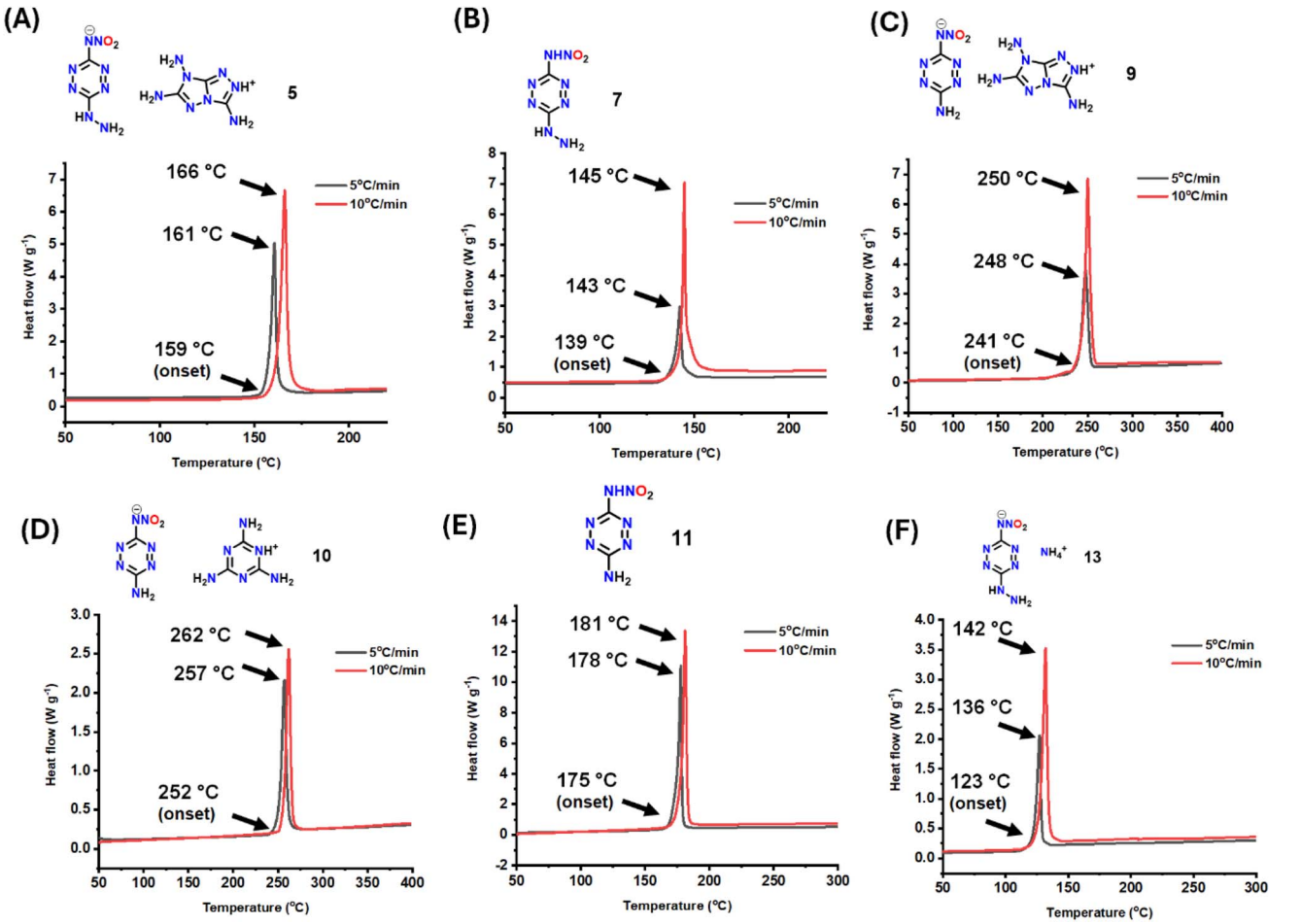

Fig. 6 DSC analysis at the heating rate of 5 °C min^{-1} and 10 °C min^{-1} (A) **5**. (B) **7**. (C) **9**. (D) **10**. (E) **11**. (F) **13**.

and N···H/H···N hydrogen bond interactions (Fig. 7E and H). The total sum of calculated populations of O···H/H···O and N···H/H···N interactions in compounds **9**·H_2O and **11** are 58% and 50%, respectively. The π-stacking between rings is visualized by plotting non-covalent interactions plots and are shown in Fig. 7F and I. A large sum of H-bond interactions in combination with π-stacking interactions enhance the thermal stability of compounds **5**, **9**·H_2O and **11**.

For compounds **5–13**, sensitivities to impact and friction were measured by using BAM standard methods and are given in Table 1. These compounds show acceptable sensitivity towards impact and friction. The sensitivities of compounds **5**, **9** and **11** are further explained from both crystal structure and at the molecular level. They have a layer-like packing pattern in the crystal structure, which when subjected to external stimuli can transform the mechanical energy into relative motion between layers. At the molecular level, sensitivities of materials toward impact are very closely related to their electrostatic potentials (ESPs). The electrostatic potentials (ESP) of compounds **5**, **7** and **11** were calculated based on the B3LYP/6-311G(d, p) method with optimized structures.[42,43] ESP minima and maxima for compounds **5**, **7**, and **11** are −82, −26, −27 kcal mol^{-1} and +107, +55, +57 kcal mol^{-1}, respectively (Fig. 8).

The densities of **5–13** were measured using a gas pycnometer at ambient temperature under a helium (He) atmosphere and range from 1.60 g cm^{-3} to 1.82 g cm^{-3} (Table 1). The enthalpies of formation of the newly synthesized compounds were calculated using the isodesmic method with the Gaussian 03 suite of programs[45] giving values for compounds **5–13** in the range from 205.5 to 1120.7 kJ mol^{-1} (Table 1). All compounds have positive enthalpies of formation owing to the presence of multiple N=N bonds. With experimental densities and calculated enthalpies of formation, detonation properties of compounds **5–13** were calculated using EXPLO5 (v7.01.01). The values of calculated detonation velocities and detonation pressures are given in Table 1 and fall between 8046–8917 m s^{-1} and 22.3–32.0 GPa, respectively, with **11** showing the highest detonation velocity and pressure. The detonation properties of compounds **5** and **11** are comparable to benchmark explosive RDX.[44]

The colors of the unsymmetrically substituted tetrazine derivatives **3–13** are shown in Fig. 9 and from pink to red to orange. In contrast with most energetic salts, compounds **7** and **11** exhibit very low solubility in water. For **7** and **11**, the explosive behavior was determined through a hot needle test, *viz.*, a red-hot (glowing) needle tapped on a 10 mg sample. Both compounds **7** and **11** show a sharp deflagration with a flame

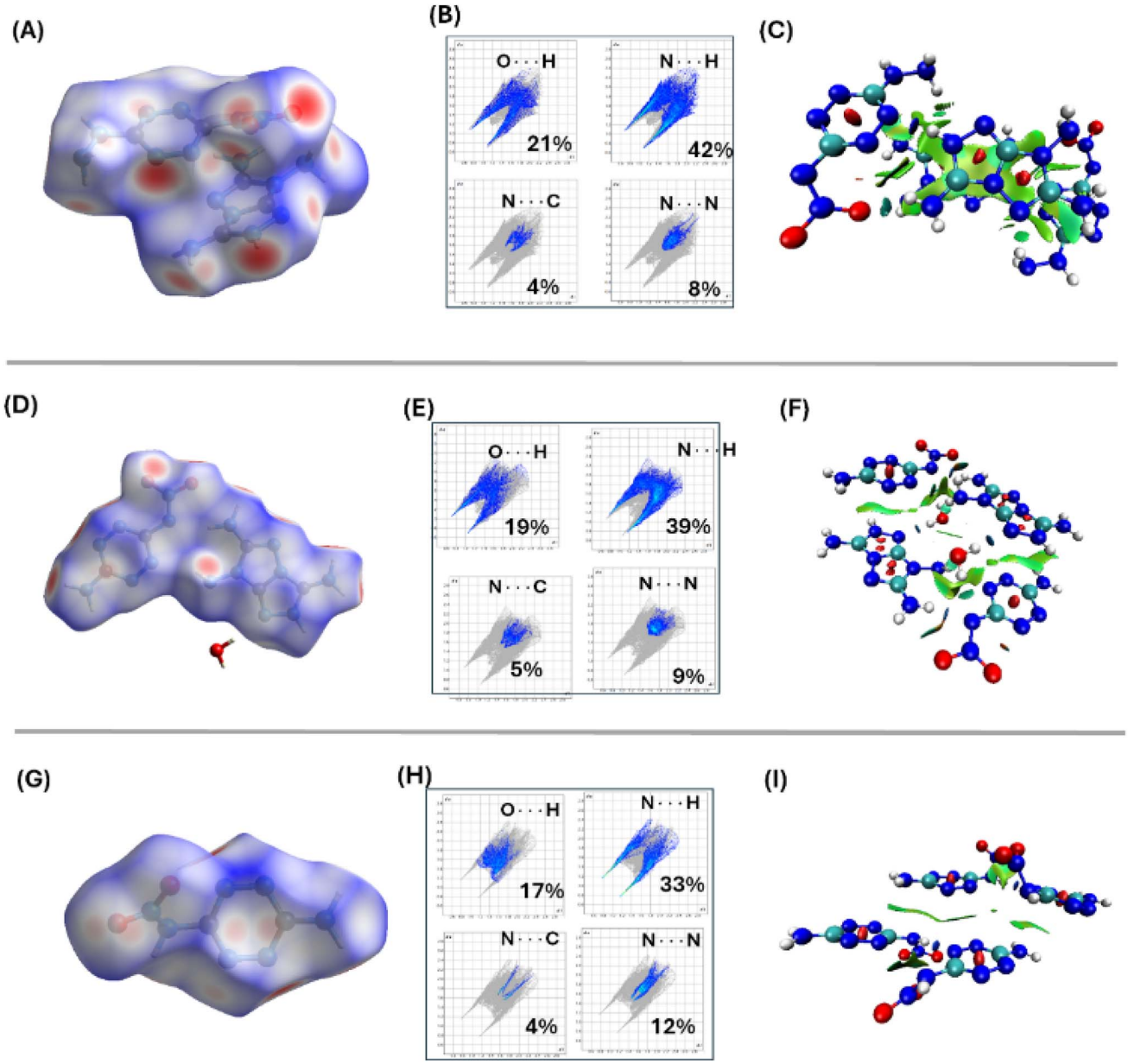

Fig. 7 (A) Hirshfeld surface of **5**. (B) 2D fingerprint plots of **5**. (C) NCI plot of **5**. (D) Hirshfeld surface of **9**·H_2O. (E) 2D fingerprint plots of **9**·H_2O. (F) NCI plot of **9**·H_2O (G) Hirshfeld surface of **11**. (H) 2D fingerprint plots of **11**. (I) NCI plot of **11**.

Table 1 Physicochemical properties of compounds **5–13**

	T_d[a] (°C)	IS[b] (J)	FS[c] (N)	ρ[d] (g cm^{-3})	ΔH_f[e] (kJmol^{-1})	D_v[f] (m s^{-1})	P[g] (GPa)	I_{sp}[h]
5	159	12	240	1.74	1120.7	8846	29.4	239
6	162	6	360	1.76	671.9	8597	26.9	212
7	139	8	120	1.75	497.6	8873	31.0	253
8	174	10	120	1.63	526.3	8713	28.6	258
9	241	25	240	1.71	1032.5	8541	27.2	236
9·H_2O	240	25	360	1.76	791.0	8810	28.9	228
10	252	25	360	1.67	584.0	7934	22.3	207
11	175	7	160	1.82	395.1	8917	32.0	245
12	135	8	240	1.62	397.7	8494	26.2	233
13	123	7	240	1.60	205.5	8046	22.8	208
RDX[i]	204	7.5	120	1.80	92.6	8795	34.9	287

[a] Temperature (onset at 5 °C min^{-1}) of decomposition. [b] Sensitivity to impact (IS). [c] Sensitivity to friction (FS). [d] Density at 25 °C using gas pycnometer. [e] Molar enthalpy of formation (calculated using isodesmic reactions with the Gaussian 03 suite of programs (revision D.01)). [f] Velocity. [g] Pressure (calculated using EXPLO5 version 7.01.01). [h] Specific impulse of neat compound calculated with EXPLO5 V 7.01.01 (I_{sp}). [i] Ref. 44.

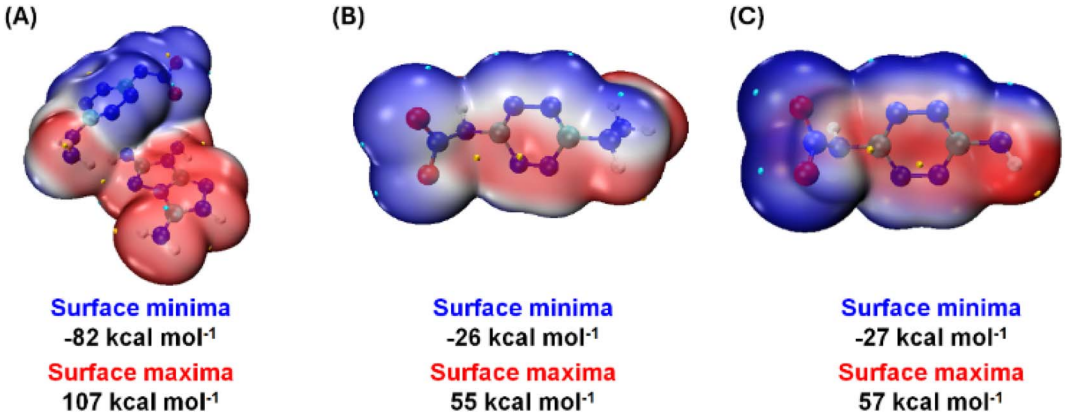

Fig. 8 ESP surfaces (A) 5. (B) 7. (C) 11.

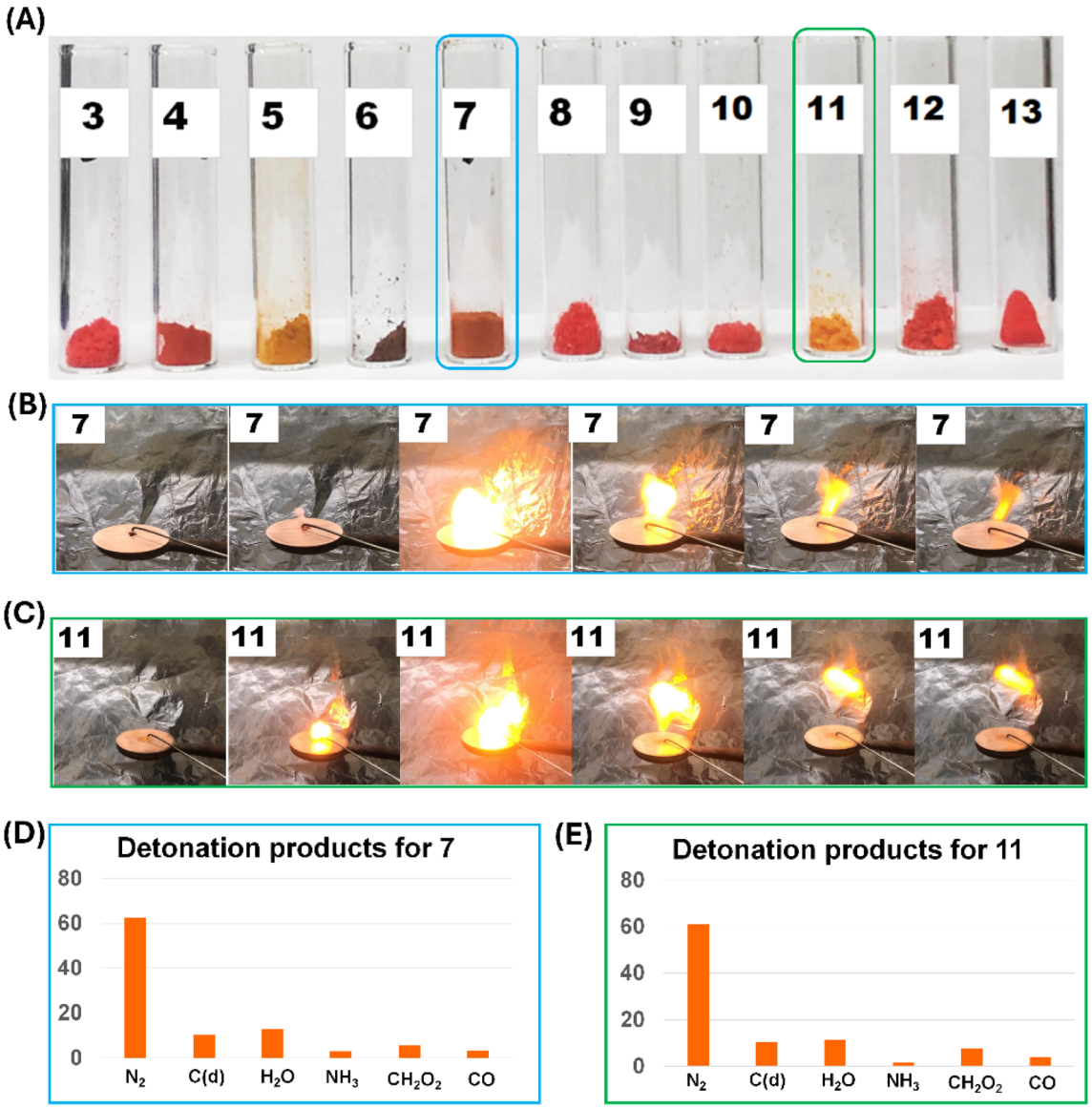

Fig. 9 (A) Colors of compounds 3–13. (B) Hot needle test for 7. (C) Hot needle test for 11. (D) Composition of detonation products for 7 [wt%]. (E) Composition of detonation products for 11 [wt%].

Table 2 Specific impulse (propulsive properties) for different high energy composite propellant formulations

	$I_{sp}{}^{a,f}$ [s]	$I_{sp}{}^{b,f}$ [s]	$I_{sp}{}^{c,f}$ [s]	$I_{sp}{}^{d,f}$ [s]	$I_{sp}{}^{e,f}$ [s]
7	253	263	244	260	234
11	245	254	238	255	231
RDX	267	278	259	268	242

[a] I_{sp} = specific impulse of neat compound (monopropellant). [b] I_{sp} = specific impulse at 88% compound and 12% Al as fuel additive. [c] I_{sp} = specific impulse at 78% compound, 12% Al, and 10% HTPB as a binder. [d] I_{sp} = specific impulse at 80% compound, 20% AP. [e] I_{sp} = specific impulse at 42% compound, 20% AP, 20% HTPB and 18% Al. [f] Specific impulse calculated at an isobaric pressure of 70 bar and initial temperature of 3300 K using EXPLO5 V 7.01.

(Fig. 9B and C). For **7** and **11**, the amount of N_2 gas released in the detonation products (calculated from the 7.01.01 version of EXPLO5) is 62% and 61%, respectively, making them environmentally friendly materials (Fig. 9D and E).

Hydrazine has traditionally played a vital role as a fuel in liquid rocket propellants, but its inherent volatility and toxicity present major hurdles in developing eco-friendly and high-performance propellants.[46] Consequently, synthesizing tetrazine derivatized with hydrazine allows for leveraging the beneficial properties of hydrazine while minimizing its toxic and volatile nature. To evaluate the applicability of **7** and **11** as solid propellants, their performance was evaluated as monopropellants (neat) and composite propellants.

The specific impulse (I_{sp}) values were calculated using EXPLO5v7.01.01 software at chamber pressure 7 MPa, expansion pressure ratio (P_c/P_e) of 70, initial T of 3500 K, ambient pressure of 0.1 MPa at the equilibrium, and expansion through the nozzle. The I_{sp} values of **7** and **11** as monopropellants (neat) are 253 s and 245 s, respectively, which is higher than AP (157 s) and ADN (206 s). Additionally, the I_{sp} values of four composite propellant formulations using **7**, **11** and RDX (i) 88% of compound and 12% Al, (ii) 78% of compound, 12% Al, and 10% HTPB. (iii) 80% compound, 20% AP (iv) 42% compound, 20% AP, 20% HTPB and 18% Al, were calculated and the results are listed in Table 2. The specific impulse values (I_{sp}) of **7** and **11** are comparable to the benchmark explosive RDX.[47,48]

3. Conclusion

In conclusion, a series of unsymmetrically substituted tetrazine derivatives was synthesized by stepwise functionalization. This study presents a feasible approach to synthesizing hydrazine/nitroamine and amino/nitroamine substituted tetrazine derivatives. The final compounds are fully characterized by $^1H/^{13}C$ NMR, and IR spectra, elemental analyses and in some cases with single crystal X-ray diffraction analysis. Energetic salts **5** and **9** exhibit good detonation properties, which are comparable to the benchmark explosive RDX. The propulsive properties observed for neutral derivatives **7** (hydrazine/nitroamine) and **11** (amino/nitroamine) highlight their significant potential for practical applications in solid propellants. This work not only advances the field of energetic materials but also opens avenues for further research and development of more sophisticated and environmentally friendly energetic compounds.

Data availability

The data underlying this study are available in the published article and its online ESI.†

Conflicts of interest

The authors declare that they have no competing financial interests or personal relationships that could have influenced the work reported in this paper.

Acknowledgements

The diffractometer (Rigaku Synergy S) for SC-XRD was purchased with support from the National Science Foundation (MRI program) under grant no. 1919565. We are grateful to the Fluorine-19 fund for support.

References

1 V. Vij, V. Bhalla and M. Kumar, *Chem. Rev.*, 2016, **116**, 9565–9627.
2 G. S. Singh, K. Mollet, M. D'Hooghe and N. De Kimpe, *Chem. Rev.*, 2013, **113**, 1441–1498.
3 A. A. Konnov, M. S. Klenov, A. M. Churakov, I. L. Dalinger, Y. A. Strelenko, I. V. Fedyanin, D. B. Lempert, A. N. Pivkina, T. S. Kon'kova, Y. N. Matyushin and V. A. Tartakovsky, *Energ. Mater. Front.*, 2023, **4**, 1–9.
4 X. Jiang, D. Yin, S. Song, Y. Wang, M. Fan, R. Wang and Q. Zhang, *J. Mater. Chem. A*, 2024, **12**, 13231–13239.
5 Y. Xu, L. Ding, D. Li, Z. Xu, P. Wang, Q. Lin and M. Lu, *J. Mater. Chem. A*, 2024, **12**, 17714–17729.
6 T. Zhu, C. Lei, C. Li, H. Yang, C. Xiao and G. Cheng, *J. Mater. Chem. A*, 2024, **12**, 4678–4683.
7 Q. Yu, J. Singh, R. J. Staples and J. M. Shreeve, *Chem. Eng. J.*, 2022, **431**, 133235.
8 Y. Dong, M. Li, G. Cheng, W. Huang, Y. Liu, C. Xiao and Y. Tang, *J. Mater. Chem. A*, 2023, **11**, 25992–25999.
9 S. Banik, P. Kumar, V. D. Ghule, S. Khanna, D. Allimuthu and S. Dharavath, *J. Mater. Chem. A*, 2022, **10**, 22803–22811.
10 S. R. Yocca, M. Zeller, E. F. C. Byrd and D. G. Piercey, *J. Mater. Chem. A*, 2022, **10**, 1876–1884.
11 J. Singh, R. J. Staples and J. M. Shreeve, *Org. Lett.*, 2023, **25**, 6082–6086.
12 J. Singh, R. J. Staples, J. P. Hooper and J. M. Shreeve, *Chem. Eng. J.*, 2022, **431**, 133282.
13 A. J. Bennett, L. M. Foroughi and A. J. Matzger, *J. Am. Chem. Soc.*, 2024, **146**, 1771–1775.
14 M. Benz, T. M. Klapotke, J. Stierstorfer and M. Voggenreiter, *J. Am. Chem. Soc.*, 2022, **144**, 6143–6147.
15 Z. Yin, W. Huang, Y. Dong, M. Li, Z. Sun, Y. Liu and Y. Tang, *J. Org. Chem.*, 2023, **88**, 14004–14011.
16 Z. Zeng, Y. Liu, G. Cheng, W. Huang, H. Wei, J. M. Shreeve and Y. Tang, *J. Mater. Chem. A*, 2021, **9**, 21685–21688.

17 L. Hu, H. Gao and J. M. Shreeve, *J. Mater. Chem. A*, 2020, **8**, 17411–17414.
18 Q. Lai, T. Fei, P. Yin and J. M. Shreeve, *Chem. Eng. J.*, 2021, **410**, 128148.
19 D. Kumar, G. H. Imler, D. A. Parrish and J. M. Shreeve, *J. Mater. Chem. A*, 2017, **5**, 16767–16775.
20 J. Tang, H. Yang, Y. Cui and G. Cheng, *Mater. Chem. Front.*, 2021, **5**, 7108–7118.
21 T. M. Klapötke and M. Suceska, *Z. Anorg. Allg. Chem.*, 2021, **647**, 572–574.
22 N. Fischer, D. Fischer, T. M. Klapötke, D. G. Piercey and J. Stierstorfer, *J. Mater. Chem.*, 2012, **22**, 20418.
23 A. K. Sikder, M. Geetha, D. B. Sarwade and J. P. Agrawal, *J. Hazard. Mater.*, 2001, **82**, 1–12.
24 D. E. Chavez, M. A. Hiskey and R. D. Gilardi, *Org. Lett.*, 2004, **6**, 2889–2891.
25 M. H. V. Huynh, M. A. Hiskey, D. E. Chavez, D. L. Naud and R. D. Gilardi, *J. Am. Chem. Soc.*, 2005, **127**, 12537–12543.
26 D. E. Chavez, B. C. Tappan, M. A. Hiskey, S. F. Son, H. Harry, D. Montoya and S. Hagelberg, *Propellants, Explos., Pyrotech.*, 2005, **30**, 412–417.
27 A. Saikia, R. Sivabalan, B. G. Polke, G. M. Gore, A. Singh, A. Subhananda Rao and A. K. Sikder, *J. Hazard. Mater.*, 2009, **170**, 306–313.
28 D. E. Chavez and D. A. Parrish, *J. Heterocycl. Chem.*, 2009, **46**, 88–90.
29 G. F. Rudakov, I. B. Kozlov, N. V. Boev, S. S. Zinchenko, L. Y. Melnikova, V. Y. Egorshev and V. P. Sinditskii, *ChemistrySelect*, 2021, **6**, 7654–7662.
30 M. D. Coburn, G. A. Buntain, B. W. Harris, M. A. Hiskey, K.-Y. Lee and D. G. Ott, *J. Heterocycl. Chem.*, 1991, **28**, 2049–2050.
31 D. E. Chavez and M. A. Hiskey, *J. Heterocycl. Chem.*, 1998, **35**, 1329–1332.
32 D. M. Bystrov, A. N. Pivkina and L. L. Fershtat, *Molecules*, 2022, **27**, 5891.
33 H. Gao, R. Wang, B. Twamley, M. A. Hiskey and J. M. Shreeve, *Chem. Commun.*, 2006, **4007**, 4007–4009.
34 G. F. Rudakov, T. V. Ustinova, I. B. Kozlov and V. F. Zhilin, *Chem. Heterocycl. Compd.*, 2014, **50**, 53–64.
35 S. Wang, X. Chen, Y. Chen, H. Nan, Y. Li and H. Ma, *Front. Chem.*, 2022, **10**, 978003.
36 Q. Liu, H. Wang, Y. Kang, Y. Liu, P. Yu, M. Yuan and H. Gao, *Energ. Mater. Front.*, 2023, **4**, 30–36.
37 X. Zhang, Y. Wang, Y. Liu, Q. Zhang, L. Hu, C. He and S. Pang, *ACS Appl. Mater. Interfaces*, 2022, **14**, 37975–37981.
38 Y. Liu, G. Zhao, Y. Tang, J. Zhang, L. Hu, G. H. Imler, D. A. Parrish and J. M. Shreeve, *J. Mater. Chem. A*, 2019, **7**, 7875–7884.
39 L. Hu, C. He, G. Zhao, G. H. Imler, D. A. Parrish and J. M. Shreeve, *ACS Appl. Energy Mater.*, 2020, **3**, 5510–5516.
40 M. A. Spackman and D. Jayatilaka, *CrystEngComm*, 2009, **11**, 19–32.
41 M. A. Spackman and J. J. McKinnon, *CrystEngComm*, 2002, **4**, 378–392.
42 T. Lu and F. Chen, *J. Comput. Chem.*, 2012, **33**, 580–592.
43 E. R. Johnson, S. Keinan, P. Mori-Sánchez, J. Contreras-García, A. J. Cohen and W. Yang, *J. Am. Chem. Soc.*, 2010, **132**, 6498–6506.
44 R. Mayer, J. Köhler and A. Homburg, *Explosives*, Wiley-VCH, 2007.
45 M. J. Frisch, G. W. Trucks, H. B. Schlegel, G. E. Scuseria, M. A. Robb, J. R. Cheeseman, G. Scalmani, V. Barone, B. Mennucci, G. A. Petersson, H. Nakatsuji, M. L. Caricato, X. Li, H. P. Hratchian, A. F. Izmaylov, J. Bloino, G. Zheng, J. L. Sonnenberg, M. Hada, M. Ehara, K. Toyota, R. Fukuda, J. Hasegawa, M. Ishida, T. Nakajima, Y. Honda, O. Kitao, H. Nakai, T. Vreven, J. A. Montgomery Jr, J. E. Peralta, F. Ogliaro, M. Bearpark, J. J. Heyd, E. Brothers, K. N. Kudin, V. N. Staroverov, R. Kobayashi, J. Normand, K. Raghavachari, A. Rendell, J. C. Burant, S. S. Iyengar, J. Tomasi, M. Cossi, N. Rega, N. J. Millam, M. Klene, J. E. Knox, J. B. Cross, V. Bakken, C. Adamo, J. Jaramillo, R. Gomperts, R. E. Stratmann, O. Yazyev, A. J. Austin, R. Cammi, C. Pomelli, J. W. Ochterski, R. L. Martin, K. Morokuma, V. G. Zakrzewski, G. A. Voth, P. Salvador, J. J. Dannenberg, S. Dapprich, A. D. Daniels, Ö. Farkas, J. B. Foresman, J. V. Ortiz, J. Cioslowski and D. J. Fox, *Revision D.01 edn*, Gaussian, Inc., Wallingford, CT, 2003.
46 M. Tang, X. Wang, X. Xu, Z. Zeng, C. Chen, Y. Liu, W. Huang and Y. Tang, *J. Mater. Chem. A*, 2024, **12**, 13081–13085.
47 T. M. Klapötke, *Chemistry of High-Energy Materials*, De Gruyter, 6th edn, 2022.
48 D. Luca, *Chemical Rocket Propulsion*, Springer Aerospace Technology, 2017.